doi:10.1016/S0022-2836(03)00271-7 J. Mol. Biol. (2003) 328, 193–204

JMB

Available online at www.sciencedirect.com

SCIENCE DIRECT®

Structural Basis for Simultaneous Binding of Two Carboxy-terminal Peptides of Plant Glutamate Decarboxylase to Calmodulin

Kyoko L. Yap[1], Tao Yuan[1], Tapas K. Mal[1], Hans J. Vogel[2] and Mitsuhiko Ikura[1]*

[1]*Division of Molecular and Structural Biology, Ontario Cancer Institute and Department of Medical Biophysics, University of Toronto, 610 University Avenue, Toronto, Ontario M5G 2M9, Canada*

[2]*Department of Biological Sciences, University of Calgary 2500 University Drive NW Calgary, Alberta T2N 1N4 Canada*

**Corresponding author*

Activation of glutamate decarboxylase (GAD) by calcium-bound calmodulin (CaM) is required for normal plant growth through regulation of γ-aminobutyrate and glutamate metabolism. The interaction of CaM with the C-terminal domain of GAD is believed to induce dimerization of the enzyme, an event implicated for Ca^{2+}-dependent enzyme activation. Here, we present the solution structure of CaM in complex with a dimer of peptides derived from the C-terminus of *Petunia hybrida* GAD. The 23 kDa ternary complex is pseudo-symmetrical with each domain of CaM bound to one of the two antiparallel GAD peptides, which form an X-shape with an interhelical angle of 60°. To accommodate the dimeric helical GAD target, the two domains of CaM adopt an orientation markedly different from that seen in other CaM–target complexes. Although the dimeric GAD domain is much larger than previously studied CaM-binding peptides, the two CaM domains appear closer together and make a number of interdomain contacts not observed in earlier complexes. The present structure of a single CaM molecule interacting with two target peptides provides new evidence for the conformational flexibility of CaM as well as a structural basis for the ability of CaM to activate two enzyme molecules simultaneously.

Keywords: calmodulin; glutamate decarboxylase; *Petunia*; dimer; NMR

Introduction

Many of the most essential events in the eukaryotic cell-cycle rely on fine-tuned intracellular calcium (Ca^{2+}) regulation for normal operation. Proteins containing the Ca^{2+}-binding EF-hand (helix-loop-helix) motif are known to be involved in mediating Ca^{2+} signal transduction, by virtue of their ability to change conformation in response to a rise in intracellular levels of Ca^{2+}. Perhaps one of the most studied of these "Ca^{2+} sensors" is calmodulin (CaM), an acidic, 148 residue protein containing four EF-hands. CaM is able to bind and regulate dozens, if not hundreds, of different target proteins, including kinases, phosphatases and ion channels.[1] Most of these interactions are Ca^{2+}-dependent, and are enabled by the presence of a hydrophobic binding surface, exposed when CaM undergoes Ca^{2+}-induced conformational change.

Ca^{2+} and CaM play critical roles in plant signal transduction pathways involved in growth regulation and response to the environment.[2] Over 30 CaM-regulated target proteins have been identified in plants. Among them is glutamate decarboxylase (GAD),[3] an enzyme that catalyzes the conversion of glutamate to CO_2 and γ-aminobutyrate (GABA). Although the enzyme is present in all mammals, yeast and *Escherichia coli*, only the plant form is known to be regulated by CaM (Figure 1).[4]

Present address: T. Yuan, Aventis Pasteur Ltd, 1755 Steeles Avenue W., Toronto, Ontario M2R 3T4, Canada.

Abbreviations used: GAD, glutamate decarboxylase; CaM, calmodulin, GABA, γ-aminobutyric acid; NMR, nuclear magnetic resonance; GADp, GAD peptide; SK2, gating domain of the small-conductance potassium channel; EF, anthrax oedema factor; HSQC, $^{1}H-^{15}N$ heteronuclear single quantum coherence; NOE, nuclear Overhauser effect; CSI, chemical shift index; NOESY, nuclear Overhauser effect spectroscopy; smMLCK, smooth muscle myosin light chain kinase; CaMKI, Ca^{2+}/CaM-dependent protein kinase I, CaMKII, Ca^{2+}/CaM-dependent protein kinase II; CaMKK, Ca^{2+}/CaM-dependent protein kinase kinase; GST, glutathione-*S*-transferase.

E-mail address of the corresponding author: mikura@uhnres.utoronto.ca

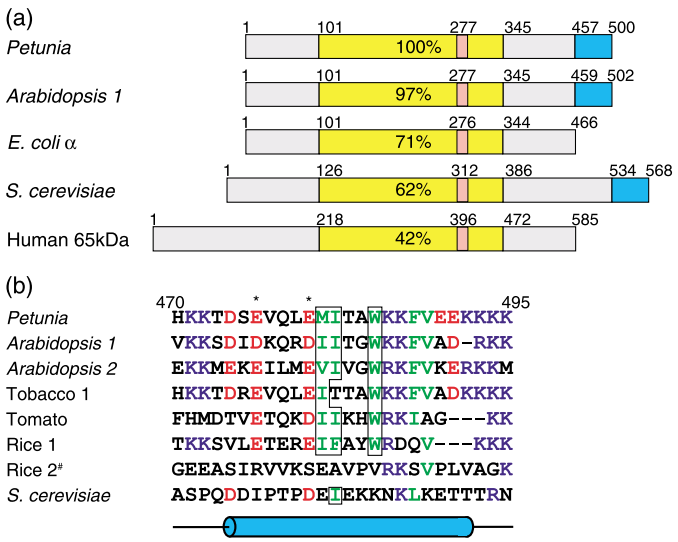

Figure 1. (a) Domain architecture of GAD from different species. Following the unconserved N-terminal domain is a structurally conserved catalytic domain (yellow) containing the pyridoxal-5′-phosphate binding site (pink). Residue numbers are indicated above the domains and percentage sequence similarities for the catalytic domains compared to *Petunia* are noted within boxes. In plant and yeast forms, there are an additional C-terminal ~50 residues comprising the CaM-binding domain (blue). *E. coli*, *Arabidopsis* and human have at least two isoforms of GAD. (b) Sequence alignment of CaM-binding domains of GAD from different species. Conserved acidic (red), basic (blue) and hydrophobic (green) residues are coloured, key anchors are boxed and potential pseudo-substrate glutamate residues are indicated with asterisks (*). The rice isoform denoted with (#) does not bind CaM. A peptide of the sequence shown for *Petunia* GAD was used in the present study with the helical region shown at bottom.

Plant GAD is the first of three enzymes in the GABA shunt, which is activated in response to stresses such as hypoxia, temperature shock, darkness and mechanical trauma.[5] These stresses lead to the accumulation of GABA and eventual stimulation of the tricarboxylic acid (Krebs) cycle. Disruption of the CaM–GAD interaction causes abnormal levels of GABA and glutamate, resulting in severe morphological deformation of the plant.[4]

Concomitant with the constant discovery of new proteins and pathways regulated by CaM, a number of NMR and X-ray crystallography structures of CaM complexes[6–14] have allowed for a better understanding of the mechanism by which CaM is able to activate such a diverse array of targets. Although these targets do not share a consensus sequence with which they bind CaM, several patterns have emerged. The classic CaM binding motif is composed of an amphipathic, single α-helix flanked by basic residues, with two bulky hydrophobic residues anchoring to each of the CaM domains.[15] The stoichiometry of the interaction is typically one molecule of CaM to one molecule of target protein, although the binding domain may be discontinuous in sequence.

In contrast, the interaction between CaM and plant GAD is atypical.[16] In addition to several lysine residues, the CaM-binding motif in *Petunia hybrida* GAD contains five acidic residues. The latter feature would appear to render it unfavorable for binding to the acidic surface of CaM. Previous *in vitro* observations of high molecular mass CaM–GAD complexes[4] and studies involving the C-terminal CaM-binding domain of GAD suggest that one molecule of CaM interacts simultaneously with two GAD peptides (GADp).[16] Here, we present the NMR-derived structure of CaM complexed with two GADp molecules. Compared to the recently determined unusual structures of CaM in complex with the gating domain of the small conductance Ca^{2+}-activated K^+ channel (SK2; one molecule of CaM binding one monomer of the dimeric channel),[12] or the anthrax oedema factor (EF; one molecule of CaM binding two subunits),[13] the interaction between CaM and GAD represents yet another multimeric mode of CaM target recognition.

Results and Discussion

Structure determination

The CaM-binding domain of GAD studied here is encompassed in a peptide comprising residues 470–495 of full-length *Petunia* GAD. The peptide is predominantly unstructured in the absence of CaM, as demonstrated by the narrow dispersion of backbone resonances in the $^1H-^{15}N$ heteronuclear single quantum coherence (HSQC) spectrum (Figure 2(a)). These observations are supported by earlier circular dichroism, fluorescence and NMR titration studies, which indicate that the peptide is largely disordered and monomeric in solution, with dimerization being induced by CaM.[16] Remarkably, addition of CaM to the GADp solution results in an increased number of peaks yet broader spectral dispersion (Figure 2(b)). This spectral change consists of (1) splitting of each individual NH resonance into a pair of peaks arising from the same NH group experiencing different chemical environments, and (2) secondary shifts on all resonances due to tertiary structure formation, together verifying the formation of a 1:2 CaM–GADp complex. Such induced-folding of a polypeptide upon complex formation with a binding protein has been observed in many cases, including other CaM–peptide,[17] KID–KIX,[18] TBP–$TAF_{II}230$[19] and Cdc42–WASP[20] complexes.

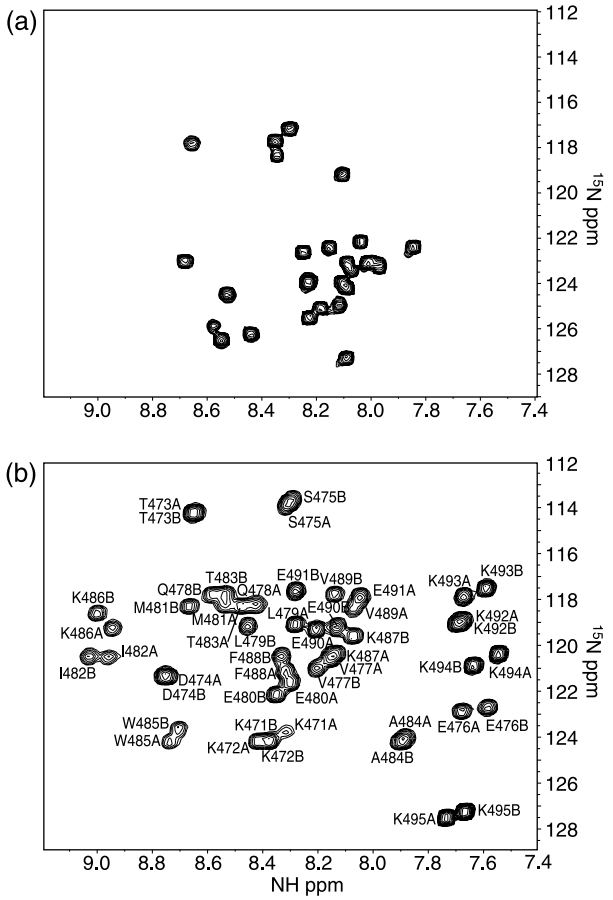

Figure 2. ^{1}H,^{15}N-HSQC spectra of GADp (a) free in solution and (b) bound to CaM. Peptide assignments for each monomer are distinguished by A or B following the residue number. The N-terminal domain of CaM binds GAD peptide B, and the C-terminal domain binds peptide A.

The complete NMR structure determination for the 23 kDa ternary complex was achieved using isotope-edited and filtered triple-resonance NMR experiments on a number of protein complex samples with various combinations of ^{15}N, ^{13}C and ^{2}H isotope labelling. Conventional methods of doubly labelling one component (CaM or GADp) of the complex yielded ^{1}H, ^{15}N and ^{13}C backbone and side-chain resonance assignments. These samples were also subject to 3D simultaneous [^{13}C,^{15}N]-edited nuclear Overhauser effect spectroscopy (NOESY)-HSQC experiments for intramolecular (CaM or GADp) NOE measurements. In application of this experiment for intra-peptide NOEs to a sample containing labelled GADp and unlabelled CaM, several NOEs from naturally abundant [^{13}C]CaM were observed. These cross-peaks were confirmed in a ^{13}C-edited, ^{13}C-filtered NOESY-HSQC experiment for labelled CaM, unlabelled GADp, which identified only NOEs between CaM and GADp. In this NOESY experiment, only NOEs between one ^{13}C-attached proton and one ^{12}C-attached proton are observed, providing key information on CaM–GADp interactions within the complex. To distinguish NOEs between the two GADp peptides from intramolecular GADp NOEs, the filtered experiment was performed on a sample containing fully deuterated CaM, equimolar ^{13}C-labelled GADp and equimolar unlabelled GADp. In this way, NOEs between CaM and GADp should not arise, since the former is deuterated, NOEs between protons on two unlabelled peptides will not be observed, while NOEs between protons on two labelled peptides should be filtered out. The remaining observable signal should arise solely between one proton on either GADp in a deuterated-CaM + (50%) ^{12}C-GADp + (50%) ^{13}C-GADp complex. From a complete backbone and side-chain resonance assignment, these two NOESY experiments (for each of CaM and GADp, and repeated with the ^{13}C carrier frequency at 67 ppm for aromatic proton NOEs) yielded 2725 distance restraints. These restraints were then combined with 359 predicted hydrogen bond and dihedral angle restraints, and 142 measured ^{1}H–^{15}N residual dipolar couplings to calculate an ensemble of structures (Table 1).

In advance of structure elucidation, ^{1}H, ^{15}N and ^{13}C resonance assignments for CaM indicated that a general fold was conserved between CaM–target complexes. Although their ^{1}H–^{15}N-HSQC spectra are not superimposable, backbone amide ^{1}H and ^{15}N chemical shifts for CaM bound to different targets[6,9,10] vary, on average, by only 0.14 ppm and 0.66 ppm, respectively, and CaM shifts from the present complex fall into these ranges (data not shown). Backbone ^{13}C shifts are also within range (average standard deviation 0.42 ppm for C^{α}, 0.45 ppm for C^{β}, 0.37 ppm for C') and the secondary structure predicted from the chemical shift index (CSI) is as observed for structures determined earlier. (As discussed below and as illustrated in Figure 5(a), the calculated structure clearly illustrates a remarkable similarity in CaM backbone conformation among various CaM–target complexes for residues 5–72 and 85–145.) However, side-chain resonances, which are more indicative of the unique adaptation of CaM to different targets, are distinct for the CaM–GADp complex from those of other complexes. Two methionine methyl resonances were extremely upfield-shifted (0.53 ppm for M71 and 0.41 ppm for M144), implying that these residues were involved strongly in interaction with GADp. Interestingly, these two methionine residues are in the same position in the two homologous (N and C) domains of CaM, suggesting that some symmetry in the CaM–GADp complex might be expected. Similarity in methyl shifts of other methionine pairs supported this possibility: 1.27 ppm and 1.36 ppm for M51 and M124, and 1.92 ppm and 1.88 ppm for M36 and M109. The most downfield methionine methyl shift belongs to M76, which is within the linker between the N and C domains. NOE patterns of other hydrophobic residues suggested formation of a symmetric complex between CaM and the two GAD peptides, or at

Table 1. Experimental restraints and structural statistics for the 20 lowest-energy structures

Number of experimental restraints	3226 (16.3 restraints/residue)[a]	
Distance restraints from NOEs	2725 (13.8 restraints/residue)[a]	
CaM[b]	1805	
GADp A, B	289, 301	
GADp A–GADp B	12	
CaM–GADp A, B	166, 162	
Dihedral angle restraints (CaM)[c]	193	
Hydrogen bond restraints[d]	166	
CaM	106	
GADp A, B	30, 30	
H–N residual dipolar coupling restraints	142	
CaM	98	
GADp A, B	22, 22	
rms Deviations from experimental data		
Average distance restraint violation (Å)	0.0137 ± 0.0065	
Average dihedral angle restraint violation (deg.)	0.3193 ± 0.0897	
Average RDC restraint violation (Å)	0.0977 ± 0.0888	
rms Deviations from ideal stereochemistry		
Bonds (Å)	0.0019 ± 0.0001	
Angles (deg.)	0.406 ± 0.014	
Impropers (deg.)	0.382 ± 0.030	
Ramachandran analysis of CaM–GADp[e]		
Residues in favored regions (%)	81.7	
Residues in additional allowed regions (%)	16.1	
Residues in generously allowed regions (%)	1.3	
Residues in disallowed regions (%)	0.9	
Coordinate precision (Å)	Backbone	All heavy-atoms
CaM, residues 12–72, 85–145	0.93 ± 0.19	1.60 ± 0.24
GADp (A, B), residues 474–492	0.52 ± 0.17	1.27 ± 0.17
CaM–GADp, residues 12–72, 85–145, 474–492	0.90 ± 0.17	1.55 ± 0.21

[a] Number of restraints per residue were calculated using CaM residues 3–148, GADp residues 470–495.
[b] Including five NOEs between the N and C-terminal domains of CaM.
[c] Predicted from TALOS.[50]
[d] Based on CSI-defined secondary structure.
[e] Performed for CaM residues 3–148 and GADp residues 470–495, excluding glycine and proline residues.

least that the interaction of one domain of CaM might interact with one peptide.

The structure of CaM bound to a dimer of GAD peptides

The solution structure of CaM complexed with two GADp molecules is well defined over most regions except for the flexible interdomain linker (residues 76–80), and the N and C termini of CaM (residues 1–7, 145–148) and GADp (residues 470–474, 493–495) (Figure 3(a) and (b)). The antiparallel peptides, which form an X, are separated by a modest distance (7.7 Å between the mid-sequence tryptophan C^{α} atoms) and intersect at 60°. Each CaM domain binds exclusively to one GADp molecule to form a pseudo-monomer that superimposes on the other with a backbone RMSD of 1.75 Å. The orientation of these monomers is therefore such that the complex appears symmetrical and compact, with a total interacting surface area of 3200 $Å^2$ between CaM and the GADp dimer (Figure 3(c)) (see Supplementary Material).

Site-directed mutagenesis of GADp demonstrated that W485 plays an essential role in the formation of the CaM–GAD complex.[21] Fluorescence experiments further suggested that the tryptophan residue from each peptide interacts directly with one of the two domains of CaM.[16] In fact, NMR data analysis indicated that NOEs arise between each GADp tryptophan residue and CaM (Figure 4(a)), as well as between the indole rings of both tryptophan residues (Figure 4(c)). This suggests that the inability of W485R GAD mutants to form complexes with CaM[21] is due to its failure to interact with the CaM domains, and its inability to form a dimer. M481 plays a similar role to W485, giving rise to strong inter-peptide and inter-CaM NOEs, while I482 is close enough to interact extensively with the hydrophobic patch of CaM, including eight of CaM's nine methionine residues. Earlier, we predicted involvement of the CaM methionine residues in GADp binding based on seleno-methionine NMR experiments.[16] Neither M481 nor I482 was considered important for complex formation in earlier biochemical studies, likely because of its proximity to W485, and the necessity

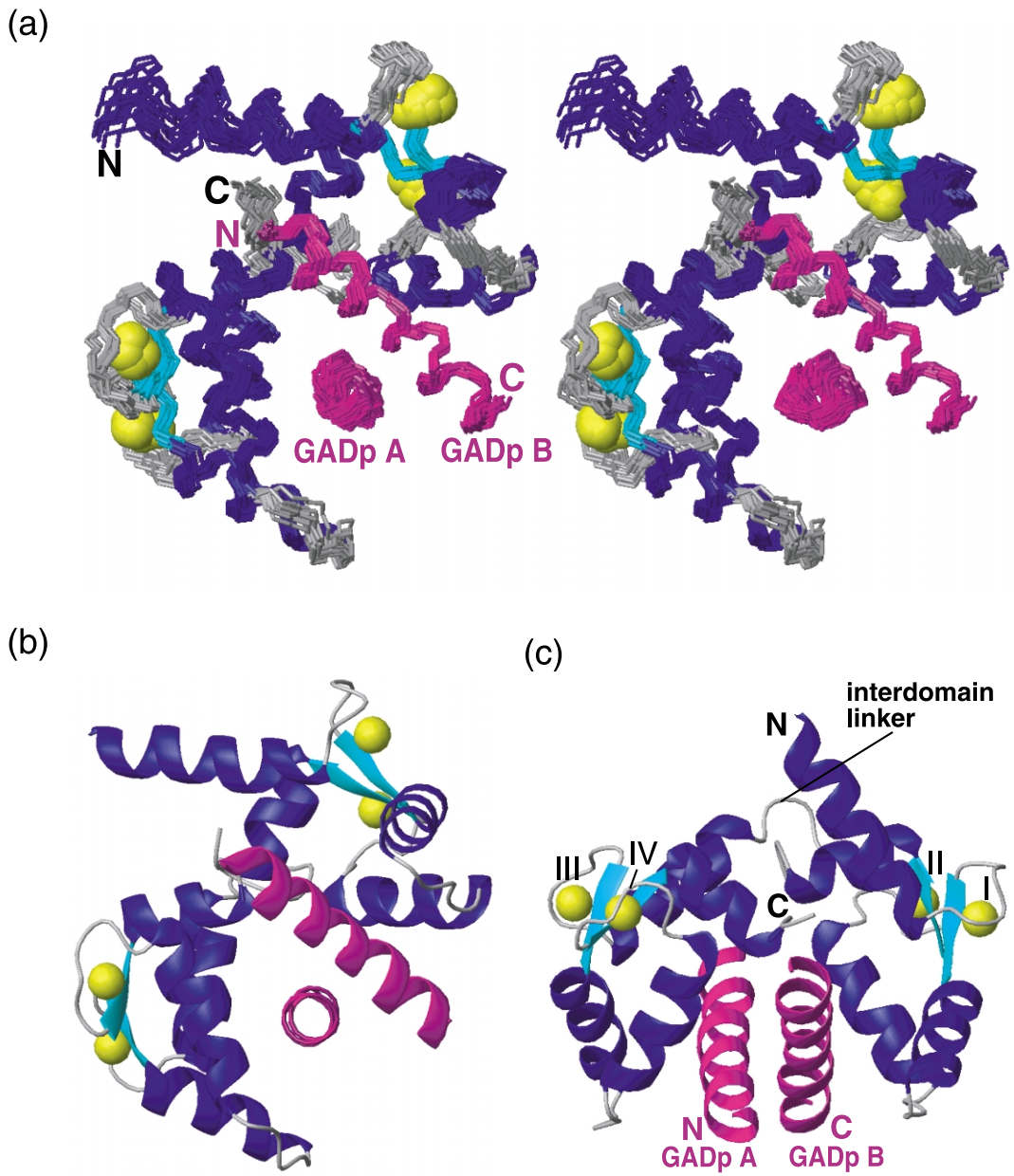

Figure 3. The NMR structure of Ca^{2+}-bound CaM in complex with GADp. (a) Stereo-view of the superposition of 20 energy-minimized structures. The view is along the axis of GAD peptide A. CaM helices are in blue, strands in cyan and calcium ions in yellow. Peptide helices are in magenta. (b) Representative structure of the 20 structures illustrated in (a). (c) Same structure rotated to illustrate its pseudo-symmetric orientation. Calcium ions are indicated with roman numerals.

of these residues for maintaining the CaM–GAD interaction is yet to be examined.

From our structure, it now appears that W485 of each peptide is not the only so-called hydrophobic anchor binding to CaM. The insertion of the I482 side-chains deep into the hydrophobic pockets of the N and C-terminal domains of CaM implies a case of two closely spaced anchors for each peptide, perhaps equivalent to a four-anchor CaM-binding sequence such as the 1-5-8-14 motif class.[15,22] The key difference for GADp is that the four hydrophobic residues belong to two molecules that bind CaM; this might be denoted, for example, as a ′1-4/1–4′ motif to illustrate interaction of two anti-parallel peptides with CaM.

In the absence of Ca^{2+}, electrostatic interactions play an essential role in forming the weaker CaM–GAD complex observed *in vitro*.[21] In the Ca^{2+}-dependent system, the interaction between CaM and GADp is predominantly hydrophobic, although cross-linking studies have shown that the deletion of the basic residues at the C terminus of GAD results in decreased affinity for CaM.[21] On the other hand, the presence of five acidic residues in the GADp sequence is an unusual feature for a CaM-binding domain, and earlier it was suggested

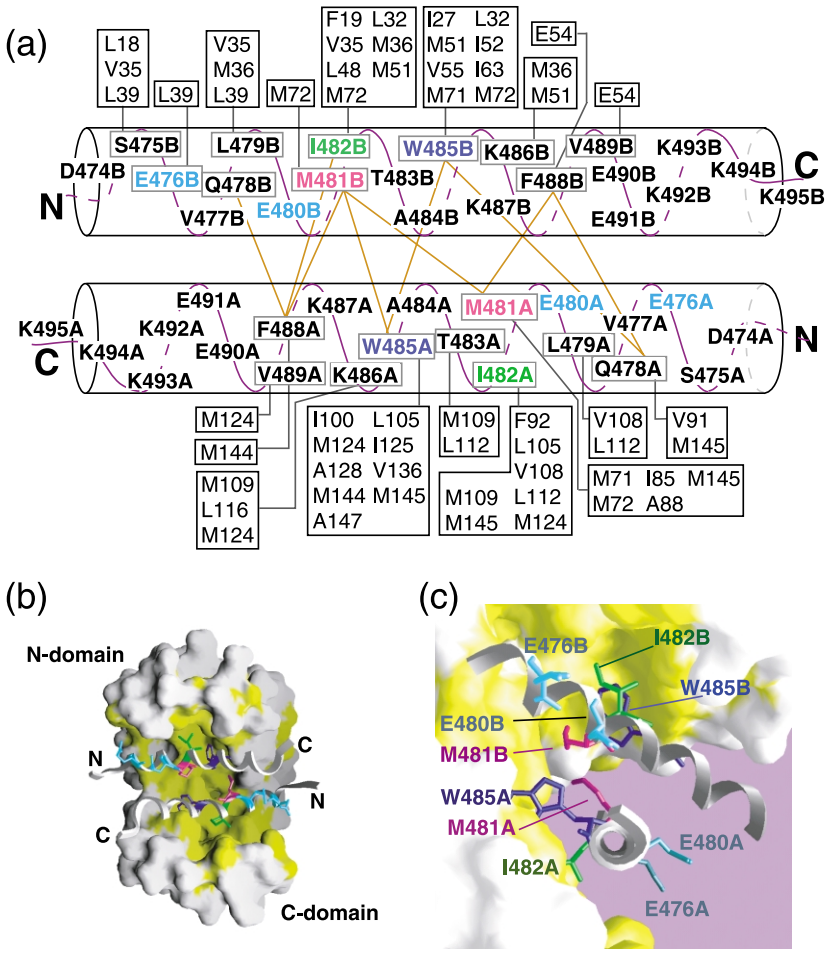

Figure 4. The interaction between CaM and GADp. (a) Schematic showing observed peptide–peptide NOEs (brown lines) and peptide–CaM NOEs (interacting CaM residues are boxed). Key interacting residues M481, I482 and W485 of GADp are coloured magenta, green and blue, respectively. Potential pseudo-substrate residues E476 and E480 are shown in cyan. (b) Surface representation of CaM showing the same orientation of peptides as in (a). Hydrophobic residues of CaM are shown in yellow. The peptide backbone ribbons and side-chains are coloured as in (a). For clarity, only GADp residues 472–493 are shown as ribbons. Note that E476 and E480 are both facing away from the CaM surface, suggesting that either residue could serve as a pseudo substrate in the absence of CaM. (c) Closer view of GADp residues interacting with the hydrophobic pockets of CaM. The structure is in the same orientation as in Figure 3(a) and (b).

that these residues might pair with basic residues on another peptide to form the dimeric interface.[16] From the present structure, the charged residues of GADp appear to be involved in both stabilizing interaction with CaM as well as building the GADp dimer interface. Specifically, one may predict the occurrence of both intramolecular (within peptide) and intermolecular (between two GADp or between GADp and CaM) electrostatic interactions based on the close proximity of these residues in the current structure, including (K487, E490), (E490, K492), (E490, K493), (E490, K494), (E491, K492) and (E491, K493) within one GAD peptide; (E480, K487) and (E480, K492) between peptides; and (E47, K486B), (D50, K486B), (E120, K486A), (E120, K487A) and (E123, K486A) between CaM and GADp (where, as in Figure 2, A denotes the GADp molecule that interacts with the C-terminal domain of CaM, B denotes the GADp molecule that interacts with the N-terminal domain). The exact geometry of these interactions, however, remains to be determined by higher-resolution methods.

Conserved residues within the homologous CaM binding domains of *Arabidopsis thaliana*, tobacco, tomato and rice GAD (Figure 1(b)) suggest that the CaM–GAD interaction in other plant species is very similar to that observed for *Petunia*. However, a recent study reported the existence of a rice GAD isoform that is unable to bind CaM.[23] This protein contains numerous substitutions in its C-terminal domain, including replacement of the key methionine, isoleucine and tryptophan residues of *Petunia* GAD with glutamate, alanine and valine, respectively. This is compelling in light of the equally poor C terminus conservation of *Saccharomyces cerevisiae* GAD, which has been shown to bind CaM *in vitro*.[24] Here, the CaM-binding I482 of *Petunia* GAD is conserved, but the peptide's dimer-mediating methionine and tryptophan residues are replaced with glutamate and lysine, respectively, suggesting an involvement of other unidentified residues in the interaction of yeast GAD with CaM.

The domain orientation of CaM in the CaM–GADp complex is affected by the large dimeric peptide volume. This volume is significantly larger (5600 Å^3) than the peptide volumes in the CaM crystal complexes with smooth muscle myosin light chain kinase peptide (smMLCKp; 1765 Å^3),[7] Ca^{2+}/CaM-dependent protein kinase I peptide (CaMKIp, 2413 Å^3),[14] Ca^{2+}/CaM-dependent protein kinase II peptide (CaMKIIp, 1611 Å^3)[8] and Ca^{2+}/CaM-dependent protein kinase kinase peptide (CaMKKp, 2275 Å^3).[11] In accommodating the larger GADp volume, CaM does not wrap around the peptides completely (Figure 4(b)), such that 3833 Å^2 of the GADp dimer remains exposed to

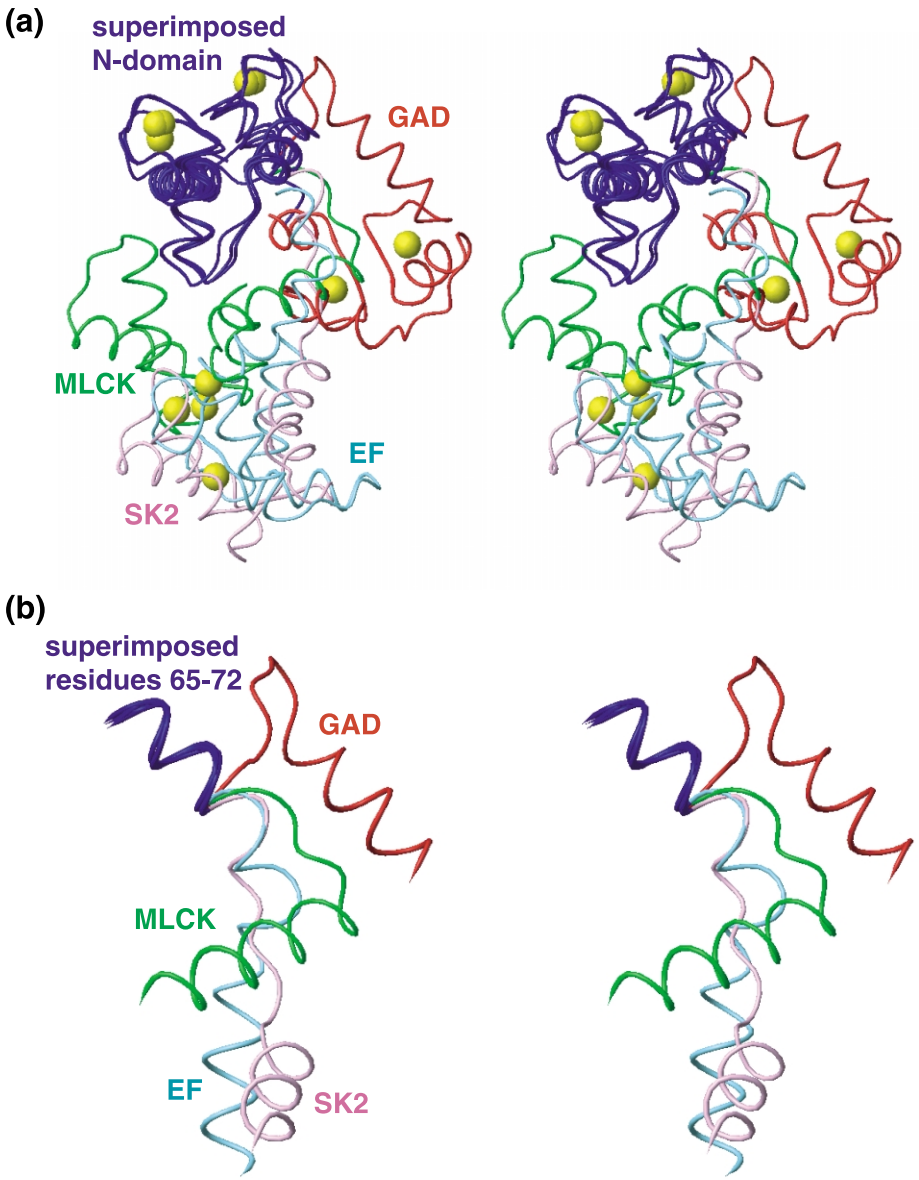

Figure 5. Comparison of CaM in different complexes clearly demonstrates uniqueness of the CaM–GADp complex. (a) Stereo-view of the superposition of the N-terminal domain of CaM when in complex with peptides from smooth muscle MLCK (1CDL)[7] (representing the CaM kinases, which superimpose with a backbone RMSD of 1.406 Å over both domains), the gating domain of Ca^{2+}-activated K^+ channel (1G4Y)[12], anthrax oedema factor (1K93)[13] and GADp. (b) Same structures, but only the interdomain linker region including helices 4 and 5 (residues 60–95) are shown. These helices may be thought of as "arrows" pointing in the direction of the N and C domains.

solvent. In spite of this, the CaM–GADp complex involves more extensive interactions between the two domains of CaM, as evidenced by a large contact surface area in the present complex (1075 $Å^2$) relative to that observed in previous CaM complexes ($<$835 $Å^2$). Interdomain NOEs were observed between residue pairs (A15, T146), (V55, E84), (A73, E82), and (A73, V142), unlike in previous studies, where NOEs occurred only between residues within the first and third EF-hands (Figure 3(c)). The proximity of the N and C-terminal helices to each other is a particularly unusual consequence of this unique domain–domain interaction. This drastic rearrangement of CaM domains is accomplished by the interdomain linker, which is highly mobile in Ca^{2+}-free and Ca^{2+}-loaded CaM, as well as in complex with various targets.[25] Interestingly, backbone $\{^1H\}-^{15}N$ NOE relaxation measurements indicate that in complex with GADp, the interdomain linker exhibits some flexibility but is more rigid compared to Ca^{2+}-loaded CaM (data not shown).

Comparison of CaM domain orientation with other target complexes

The novel orientation of the domains of CaM in the CaM–GADp complex is readily appreciated in

Table 2. Comparison of CaM–GADp complex structure with other CaM–target complexes

	GADp	MLCKp	CaMKIp	CaMKIIp	CaMKKp	EF	SK2
Peptide volume (Å^3)	5600	1765	2413	1611	2275	[a]	[a]
CaM N (residues 1–78) and C domain (79–148) interacting area (Å^2)	1075	778	832	446	731	362	153
Interhelical angle between CaM helices 4 (residues 65–72) and 5 (85–92)	−17.2	−114.2	117.8[b]	−123.2	−115.3	47.8	78.0
VGM[c] θ (180° − interhelical angle)	162.0	67.0	62.5	58.3	66.2	129.4	101.2
VGM ϕ	62.9	21.0	36.3	10.0	16.8	2.0	57.7
Distance between CaM residues 72 and 85 (Å)	13.5	17.6	19.4	20.1	18.6	25.1	28.9
Total (CaM + target) interacting surface area (Å^2)	3149	2789	3340	2491	3143	5468	2400 4536[d]

[a] Full-length domain or protein.
[b] Due to its position slightly counter-clockwise from the other CaM kinase helix pairs, this angle is designated as negative.
[c] Vector geometry mapping values calculated as described.[59] The reference is EF-hand 1 of apo-CaM (1DMO)[61] as described.[62]
[d] The first value is for CaM + one monomer of the gating domain of SK2; the second value is for CaM + dimer. The full complex contains two CaM molecules bound to the dimer.

a direct comparison with previously determined CaM complex crystal structures (Figure 5(a) and Table 2). When one domain of CaM is used as the basis for superposition (with an RMSD of 0.63 Å for N-terminal residues 12–72 of CaM in complex with smMLCKp, CaMKIp, CaMKIIp, CaMKKp, SK2 and GADp; 0.70 Å for C-terminal residues 85–145 in smMLCKp, CaMKIp, CaMKIIp, CaMKKp, EF and GADp complexes), the other domain assumes an orientation unique to its target. The overall conformations of CaM bound to various CaM kinase peptides are relatively similar to each other, conforming to the classic CaM–peptide binding motifs.[15,26] When bound to SK2[12] or EF[13], the CaM domains are in a much more extended orientation to accommodate their longer, discontinuous binding sequence lacking the conventional CaM-binding pattern. CaM in the GADp complex appears to provide yet another unique structure in this comparison, as the sharp turn in the interdomain linker brings the two domains of CaM in proximity to each other. This is especially evident when comparing the angles between the helices flanking the linker: For helices spanning residues 65–72 and 85–92 (Figure 5(b)), the interhelical angle for the CaM kinase peptide complexes range between −114.2° and −123.2°; 78.0° for the SK2 complex, 47.8° for EF, and −26.3° for GADp. Similarly, the distance between residues 72 and 85 illustrates the domain compactness of the CaM–GADp complex: These residues are separated by 13.5 Å in the case of GADp, significantly shorter than that for the CaM kinase peptides (17.6–20.1 Å), SK2 (28.9 Å) or EF (25.1 Å).

Role of CaM in GAD activation

In the absence of CaM, many CaM-activated enzymes, such as the CaM kinases, are autoinhibited by a regulatory domain consisting of "pseudo-substrate" and CaM-binding regions. The binding of CaM promotes the release of the regulatory domain from the catalytic domain, thereby activating the enzyme.[17] Several lines of evidence suggest that plant GAD employs this autoinhibition mechanism for activation. First, CaM stimulates enzyme activity (for *Petunia*, by over 20-fold).[27] Second, addition of the CaM antagonist trifluoperazine and the Ca^{2+}-chelator EGTA has a significant effect on full-length GAD activity but not on the constitutive activity of mutant GAD lacking the C-terminal CaM binding domain.[4] Third, a monoclonal antibody for the CaM-binding domain of GAD was able to activate the enzyme in the absence of CaM.[27] Taken together, these data suggest that binding of CaM to the C-terminal domain of GAD likely releases an unidentified autoinhibition region from the catalytic domain, and that GADp represents an appropriate model to study the physical interaction between CaM and GAD, as seen in many CaM-dependent enzymes such as MLCK, CaMKII and calcineurin.[17]

In light of the extensive charcterization of the regulatory mechanism of CaM kinases and other CaM-dependent enzymes,[28] it is tempting to speculate that the autoinhibitory region is located near the CaM-binding domain in GAD. Interestingly, the CaM-binding region in all plant GAD is rich in glutamate and aspartate (Figure 1(b)), amino acids that could serve as an internal pseudo-substrate for the enzyme. The most plausible candidates for this pseudo-substrate residue in *Petunia* are E476 and E480 (Figure 4(b) and (c)), which are both highly conserved among different species in plants (Figure 1(b)). As these residues are within the CaM-binding domain, the autoinhibition of the enzyme can be suppressed easily by CaM binding as a consequence of release of this portion from the catalytic domain. It should be noted that there are other candidates for pseudo-substrate residues in plant GAD (E423, E431, or E443 in *Petunia*), which are all well conserved among different species and isoforms but located approximately 25–50 residues upstream from the CaM-binding domain.

Although plant GAD may use an activation mechanism similar to that of the CaM kinases, there is an obvious difference: in CaM kinases and

other CaM-dependent enzymes, the stoichiometry of the CaM–target interaction is typically 1:1. In contrast, our previous study[16] and the present structure indicate clearly that one CaM molecule can simultaneously clamp the C-terminal tail of two GAD molecules, implying cooperative activation of two GAD enzymes by a single CaM molecule. This might represent a more economical way for GAD to respond to Ca^{2+} fluxes induced in the plant cell by external stimuli. In *Petunia* and other plants, GAD is a ubiquitously expressed, relatively abundant CaM-binding protein, which may exceed the concentration of CaM to varying degrees depending on tissue and organ type.[4,29,30]

The structurally conserved, ~240 residue catalytic domain found in GAD across all species contains a consensus sequence for binding the cofactor pyridoxal-5′-phosphate (Figure 1).[31,32] This region has been predicted to include the dimerization interface of mammalian GAD.[33] *E. coli* GAD, which is 63% homologous to *Petunia* GAD over its full-length sequence but lacks the CaM-binding domain, appears to be oligomeric.[34] Additionally, it has been shown that fully active plant GAD exists as a >500 kDa complex containing both CaM and GAD.[4] Since other oligomeric CaM-dependent enzymes exist, such as CaMKII and smMLCK, it is of interest to speculate two possible scenarios for CaM stimulation of plant GAD. First, plant GAD may form an obligatory multimeric complex independent of CaM binding. As discussed above, binding of CaM would then induce the removal of the regulatory domain from the catalytic domain, leading to an elevation of enzyme activity. However, unlike other known cases, only one CaM molecule would be required to activate two GAD molecules. The second scenario involves the CaM-dependent dimerization as part of the oligomerization of the enzyme. Here, CaM binding to GAD would promote the release of the autoinhibition and would help in the assembly of the fully active multimeric structure. It remains to be seen if the activity of GAD can be stimulated *in vitro* when only one molar equivalent of GAD is available to bind to CaM. Further biochemical and structural studies are needed to better define the mechanism underlying CaM-dependent GAD activation.

Materials and Methods

Sample preparation

^{15}N,^{13}C-labelled, ^{15}N-labelled and unlabelled *Xenopus laevis* CaM were expressed and purified as described.[35] Mammalian CaM is 89% identical with and 97% similar to either of the two CaM isoforms found in *Petunia*, and has been demonstrated to form viable, active complexes with full-length GAD (K_d 15 nM) *in vitro*.[27] ^{15}N,^{13}C-labelled and ^{13}C-labelled peptides corresponding to the CaM-binding domain in *Petunia* GAD (*GS* HKKTDS EVQLEMITAWKKFVEEKKKK) were overexpressed in *E. coli* BL21(DE3) cells as glutathione-*S*-transferase (GST) fusion constructs. The N-terminal G-S is derived from the thrombin digestion site on the vector, and resonances for these residues were not observed in recorded spectra, presumably due to fast hydrogen exchange rates. The GST tag was removed by thrombin digestion according to the manufacturer's directions (Amersham Biosciences, Piscataway, NJ). Peptide purity was verified by mass spectrometry and $^{1}H-^{15}N$-HSQC NMR experiments. Unlabelled GAD peptide (residues H470-K495) was synthesized with a solid-phase peptide synthesizer (Queen's University Peptide Synthesis Laboratory, Kingston ON, Canada). The concentrations of CaM and GAD peptide solutions were measured by ultraviolet spectroscopy as described.[16] Titration of GAD peptide into CaM solution until complex saturation was monitored by peak changes observed in the ^{1}H,^{15}N-HSQC spectrum. All NMR samples contained at least 1.0 mM CaM and 2.2 mM GADp (to ensure complex saturation) in 100 mM KCl, 10 mM $CaCl_2$, 0.2 mM NaN_3 and 91% H_2O/9% $^{2}H_2O$ at pH 6.3. Four CaM–GADp samples with different combinations of isotope labelling were used for NMR experiments: Sample A, ^{15}N-labelled CaM complexed with unlabelled GADp; sample B, ^{15}N,^{13}C-labelled CaM complexed with unlabelled GADp; sample C, unlabelled CaM complexed with ^{15}N,^{13}C-labelled GADp; sample D, ^{15}N,(99%)^{2}H-CaM complexed with 50% ^{13}C-labelled GADp, 50% unlabelled GADp. For residual dipolar coupling measurements, samples were aligned using 10 mg Pf1 phage (Asla Labs, Latvia) per 500 μl volume.

NMR spectroscopy

All NMR data were acquired at 35 °C on Varian UnityPlus 500 MHz and 600 MHz spectrometers equipped with 5 mm triple-resonance probes with *XYZ*-gradients and operating at proton frequencies of 496.812 MHz and 600.256 MHz, respectively. All experiments employed a spectral width of 13 ppm for ^{1}H. For calmodulin and GAD peptide assignments, backbone resonances were obtained from ^{1}H,^{15}N-HSQC,[36] HNCACB,[36] CBCA(CO)NH[37] and HNCO[36] experiments using samples A, B and C; side-chain resonances were obtained from ^{1}H,^{13}C-HSQC,[38] HCCH-TOCSY,[39] CCC-TOCSY-NNH,[40] HCC-TOCSY-NNH,[40] (HB)CB(CGCD)HD[41] and (HB)CB(CGCE)HE[41] experiments with samples B and C; NOE assignments from 3D simultaneous ^{13}C,^{15}N-edited NOESY-HSQC[42] (samples B and C) and ^{13}C-edited, ^{13}C-filtered NOESY-HSQC[43,44] experiments (samples B and C for NOEs between CaM and GADp; sample D for NOEs between GADp); and dipolar coupling measurements from in-phase/anti-phase (IPAP)-(^{1}H,^{15}N)-HSQC[45] experiments using samples B and C with added phage. The mixing time for all NOESY experiments was 150 ms and experiments were acquired with carrier frequencies at 43 ppm and 67 ppm for aromatic resonances. The 3D simultaneous ^{13}C,^{15}N-edited NOESY-HSQC was recorded with (128, 32, 832) complex points and (t_1, t_2, t_3) acquisition times of (21.3 ms, 6.7 ms, 53.3 ms) for both CaM and GADp measurements; the ^{13}C-edited, ^{13}C-filtered NOESY-HSQC was recorded with (80, 32, 960) and (56, 30, 960) complex points and (t_1, t_2, t_3) acquisition times of (13.3 ms, 8.9 ms, 61.5 ms) and (9.3 ms, 8.3 ms, 61.5 ms) for CaM and GADp, respectively. All data were processed with nmrPipe.[46]

Structure calculation

All spectra were analyzed using XEASY and SPSCAN.[47] Initial structures were calculated with DYANA[48] using distance restraints obtained by NOESY experiments, hydrogen bond restraints based on secondary structure defined by an in-house modification of the CSI,[49] and dihedral angle restraints predicted by TALOS.[50] Further calculations and refinement with inclusion of residual dipolar couplings[51] were performed by a mixed Cartesian and torsion angle simulated annealing protocol in CNS.[52] The 20 lowest-energy structures from a total of 200 calculated were selected and subjected to conjugate gradient minimization using the AMBER forcefield[53] in InsightII (Accelrys Inc, San Diego CA). Structures were visualized with MOLMOL,[54] Molscript,[55] Raster3D[56] and GRASP,[57] and evaluated with PROCHECK.[58] Interhelical angles and distances were calculated by VGM,[59] molecular volumes by GRASP, interacting surface areas by the Protein–Protein Interaction Server[60] and solvent-accessible surfaces by NACCESS†.

Data Bank accession codes

Resonance assignments have been deposited in the BioMagResBank with accession code 7224. NOE distance restraints and atomic coordinates have been deposited in the RCSB Protein Data Bank with accession code 1NWD.

Acknowledgements

We thank Hillel Fromm at the University of Leeds for generously providing original GAD cDNA constructs, Claude Klee at the NIH for providing the original *Xenopus* CaM expression vector, and Kit Tong for excellent technical assistance. This work was supported by Canadian Institutes of Health and Research (CIHR) grants to M.I. and H.J.V., a CIHR fellowship to K.L.Y. and National Cancer Institute of Canada fellowships to T.Y. and T.K.M. M.I. is a CIHR Investigator and H.J.V. is an Alberta Heritage Foundation for Medical Research (AHFMR) Senior Scientist.

References

1. Chin, D. & Means, A. R. (2000). Calmodulin: a prototypical calcium sensor. *Trends Cell. Biol.* **10**, 322–328.
2. Snedden, W. A. & Fromm, H. (1998). Calmodulin, calmodulin-related proteins and plant responses to the environment. *Trends Plant Sci.* **3**, 299–304.
3. Baum, G., Chen, Y., Arazi, T., Takatsuji, H. & Fromm, H. (1993). A plant glutamate decarboxylase containing a calmodulin binding domain. Cloning, sequence, and functional analysis. *J. Biol. Chem.* **268**, 19610–19617.
4. Baum, G., Lev-Yadun, S., Fridmann, Y., Arazi, T., Katsnelson, H., Zik, M. & Fromm, H. (1996). Calmodulin binding to glutamate decarboxylase is required for regulation of glutamate and GABA metabolism and normal development in plants. *EMBO J.* **15**, 2988–2996.
5. Shelp, B. J., Bown, A. W. & McLean, M. D. (1999). Metabolism and functions of gamma-aminobutyric acid. *Trends Plant Sci.* **4**, 446–452.
6. Ikura, M., Clore, G. M., Gronenborn, A. M., Zhu, G., Klee, C. B. & Bax, A. (1992). Solution structure of a calmodulin-target peptide complex by multidimensional NMR. *Science*, **256**, 632–638.
7. Meador, W. E., Means, A. R. & Quiocho, F. A. (1992). Target enzyme recognition by calmodulin: 2.4 Å structure of a calmodulin–peptide complex. *Science*, **257**, 1251–1255.
8. Meador, W. E., Means, A. R. & Quiocho, F. A. (1993). Modulation of calmodulin plasticity in molecular recognition on the basis of x-ray structures. *Science*, **262**, 1718–1721.
9. Osawa, M., Tokumitsu, H., Swindells, M. B., Kurihara, H., Orita, M., Shibanuma, T. *et al.* (1999). A novel target recognition revealed by calmodulin in complex with Ca^{2+}-calmodulin-dependent kinase kinase. *Nature Struct. Biol.* **6**, 819–824.
10. Elshorst, B., Hennig, M., Forsterling, H., Diener, A., Maurer, M., Schulte, P. *et al.* (1999). NMR solution structure of a complex of calmodulin with a binding peptide of the Ca^{2+} pump. *Biochemistry*, **38**, 12320–12332.
11. Kurokawa, H., Osawa, M., Kurihara, H., Katayama, N., Tokumitsu, H., Swindells, M. B. *et al.* (2001). Target-induced conformational adaptation of calmodulin revealed by the crystal structure of a complex with nematode Ca^{2+}/calmodulin-dependent kinase kinase peptide. *J. Mol. Biol.* **312**, 59–68.
12. Schumacher, M. A., Rivard, A. F., Bachinger, H. P. & Adelman, J. P. (2001). Structure of the gating domain of a Ca^{2+}-activated K^+ channel complexed with Ca^{2+}/calmodulin. *Nature*, **410**, 1120–1124.
13. Drum, C. L., Yan, S. Z., Bard, J., Shen, Y. Q., Lu, D., Soelaiman, S. *et al.* (2002). Structural basis for the activation of anthrax adenylyl cyclase exotoxin by calmodulin. *Nature*, **415**, 396–402.
14. Clapperton, J. A., Martin, S. R., Smerdon, S. J., Gamblin, S. J. & Bayley, P. M. (2002). Structure of the complex of calmodulin with the target sequence of calmodulin-dependent protein kinase I: studies of the kinase activation mechanism. *Biochemistry*, **41**, 14669–14679.
15. Yap, K. L., Kim, J., Truong, K., Sherman, M., Yuan, T. & Ikura, M. (2000). Calmodulin target database. *J. Struct. Funct. Genom.* **1**, 8–14.
16. Yuan, T. & Vogel, H. J. (1998). Calcium-calmodulin-induced dimerization of the carboxyl-terminal domain from petunia glutamate decarboxylase. A novel calmodulin–peptide interaction motif. *J. Biol. Chem.* **273**, 30328–30335.
17. Crivici, A. & Ikura, M. (1995). Molecular and structural basis of target recognition by calmodulin. *Annu. Rev. Biophys. Biomol. Struct.* **24**, 85–116.
18. Parker, D., Jhala, U. S., Radhakrishnan, I., Yaffe, M. B., Reyes, C., Shulman, A. I. *et al.* (1998). Analysis of an activator:coactivator complex reveals an essential role for secondary structure in transcriptional activation. *Mol. Cell*, **2**, 353–359.
19. Liu, D., Ishima, R., Tong, K. I., Bagby, S., Kokubo, T., Muhandiram, D. R. *et al.* (1998). Solution structure of a TBP-TAF(II)230 complex: protein mimicry of

† http://wolf.bms.umist.ac.uk/naccess/

the minor groove surface of the TATA box unwound by TBP. *Cell*, **94**, 573–583.
20. Kim, A. S., Kakalis, L. T., Abdul-Manan, N., Liu, G. A. & Rosen, M. K. (2000). Autoinhibition and activation mechanisms of the Wiskott–Aldrich syndrome protein. *Nature*, **404**, 151–158.
21. Arazi, T., Baum, G., Snedden, W. A., Shelp, B. J. & Fromm, H. (1995). Molecular and biochemical analysis of calmodulin interactions with the calmodulin-binding domain of plant glutamate decarboxylase. *Plant Physiol.* **108**, 551–561.
22. Rhoads, A. R. & Friedberg, F. (1997). Sequence motifs for calmodulin recognition. *FASEB J.* **11**, 331–340.
23. Akama, K., Akihiro, T., Kitagawa, M. & Takaiwa, F. (2001). Rice (*Oryza sativa*) contains a novel isoform of glutamate decarboxylase that lacks an authentic calmodulin-binding domain at the C-terminus. *Biochim. Biophys. Acta*, **1522**, 143–150.
24. Coleman, S. T., Fang, T. K., Rovinsky, S. A., Turano, F. J. & Moye-Rowley, W. S. (2001). Expression of a glutamate decarboxylase homologue is required for normal oxidative stress tolerance in *Saccharomyces cerevisiae*. *J. Biol. Chem.* **276**, 244–250.
25. Barbato, G., Ikura, M., Kay, L. E., Pastor, R. W. & Bax, A. (1992). Backbone dynamics of calmodulin studied by ^{15}N relaxation using inverse detected two-dimensional NMR spectroscopy: the central helix is flexible. *Biochemistry*, **31**, 5269–5278.
26. Hoeflich, K. P. & Ikura, M. (2002). Calmodulin in action: diversity in target recognition and activation mechanisms. *Cell*, **108**, 739–742.
27. Snedden, W. A., Koutsia, N., Baum, G. & Fromm, H. (1996). Activation of a recombinant petunia glutamate decarboxylase by calcium/calmodulin or by a monoclonal antibody which recognizes the calmodulin binding domain. *J. Biol. Chem.* **271**, 4148–4153.
28. Hook, S. S. & Means, A. R. (2001). Ca^{2+}/CaM-dependent kinases: from activation to function. *Annu. Rev. Pharmacol. Toxicol.* **41**, 471–505.
29. Zielinski, R. E. (1998). Calmodulin and calmodulin-binding proteins in plants. *Annu. Rev. Plant Physiol. Plant Mol. Biol.* **41**, 471–505.
30. Chen, Y., Baum, G. & Fromm, H. (1994). The 58-kilodalton calmodulin-binding glutamate decarboxylase is a ubiquitous protein in petunia organs and its expression is developmentally regulated. *Plant Physiol.* **106**, 1381–1387.
31. Qu, K., Martin, D. L. & Lawrence, C. E. (1998). Motifs and structural fold of the cofactor binding site of human glutamate decarboxylase. *Protein Sci.* **7**, 1092–1105.
32. Areshev, A. G., Mamaeva, O. K., Andreeva, N. S. & Sukhareva, B. S. (2000). Structure of glutamate decarboxylase and related PLP-enzymes: computer-graphical studies. *J. Biomol. Struct. Dynam.* **18**, 127–136.
33. Schwartz, H. L., Chandonia, J. M., Kash, S. F., Kanaani, J., Tunnell, E., Domingo, A. *et al.* (1999). High-resolution autoreactive epitope mapping and structural modeling of the 65 kDa form of human glutamic acid decarboxylase. *J. Mol. Biol.* **287**, 983–999.
34. Sukhareva, B. S., Tikhonenko, A. S. & Darii, E. L. (1994). Examination of quaternary strucxture of *Escherichia coli* glutamate decarboxylase. *Mol. Biol.* **28**, 874–876.
35. Ikura, M., Kay, L. E. & Bax, A. (1990). A novel approach for sequential assignment of ^{1}H, ^{13}C, and ^{15}N spectra of proteins: heteronuclear triple-resonance three-dimensional NMR spectroscopy. Application to calmodulin. *Biochemistry*, **29**, 4659–4667.
36. Muhandiram, D. R. & Kay, L. E. (1994). Gradient-enhanced triple-resonance three-dimensional NMR experiments with improved sensitivity. *J. Magn. Reson. ser. B*, **103**, 203–216.
37. Grzesiek, S. & Bax, A. (1992). Correlating backbone amide and side-chain resonances in larger proteins by multiple relayed triple resonance NMR. *J. Am. Chem. Soc.* **114**, 6291–6293.
38. Vuister, G. & Bax, A. (1992). Resolution enhancement and spectral editing of uniformly ^{13}C-enriched proteins by homonuclear broadband ^{13}C decoupling. *J. Magn. Reson.* **98**, 428–435.
39. Bax, A., Clore, G. M. & Gronenborn, A. M. (1990). 1H–1H correlation *via* isotropic mixing of ^{13}C magnetization, a new three-dimensional approach for assigning 1H and ^{13}C spectra of ^{13}C-enriched proteins. *J. Magn. Reson.* **88**, 425–431.
40. Grzesiek, S., Anglister, J. & Bax, A. (1993). Correlation of backbone amide and aliphatic side-chain resonances in ^{13}C/^{15}N-enriched proteins by isotropic mixing of 13C magnetization. *J. Magn. Reson. ser. B*, **101**, 114–119.
41. Yamazaki, T., Forman-Kay, J. D. & Kay, L. E. (1993). Two-dimensional NMR experiments for correlating ^{13}C-beta and ^{1}H-delta/epsilon chemical shifts of aromatic residues in ^{13}C-labeled proteins *via* scalar couplings. *J. Am. Chem. Soc.* **115**, 11054–11055.
42. Pascal, S. M., Muhandiram, D. R., Yamazaki, T., Forman-Kay, J. D. & Kay, L. E. (1994). Simultaneous acquisition of ^{15}N-edited and ^{13}C-edited NOE spectra of proteins dissolved in H_2O. *J. Magn. Reson. ser. B*, **103**, 197–201.
43. Lee, W., Revington, M. J., Arrowsmith, C. & Kay, L. E. (1994). A pulsed field gradient isotope-filtered 3D ^{13}C HMQC-NOESY experiment for extracting intermolecular NOE contacts in molecular complexes. *FEBS Letters*, **350**, 87–90.
44. Tomomori, C., Tanaka, T., Dutta, R., Park, H., Saha, S. K., Zhu, Y. *et al.* (1999). Solution structure of the homodimeric core domain of *Escherichia coli* histidine kinase EnvZ. *Nature Struct. Biol.* **6**, 729–734.
45. Goto, N. K., Skrynnikov, N. R., Dahlquist, F. W. & Kay, L. E. (2001). What is the average conformation of bacteriophage T4 lysozyme in solution? A domain orientation study using dipolar couplings measured by solution NMR. *J. Mol. Biol.* **308**, 745–764.
46. Delaglio, F., Grzesiek, S., Vuister, G. W., Zhu, G., Pfeifer, J. & Bax, A. (1995). NMRPipe: a multi-dimensional spectral processing system based on UNIX pipes. *J. Biomol. NMR*, **6**, 277–293.
47. Bartels, C., Xia, T.-H., Billeter, M., Guntert, P. & Wuthrich, K. (1995). The program XEASY for computer-supported NMR spectral-analysis of biological macromolecules. *J. Biomol. NMR*, **5**, 1–10.
48. Guntert, P., Mumenthaler, C. & Wuthrich, K. (1997). Torsion angle dynamics for NMR structure calculation with the new program DYANA. *J. Mol. Biol.* **273**, 283–298.
49. Wishart, D. S. & Sykes, B. D. (1994). The ^{13}C chemical-shift index: a simple method for the identification of protein secondary structure using ^{13}C chemical-shift data. *J. Biomol. NMR*, **4**, 171–180.
50. Cornilescu, G., Delaglio, F. & Bax, A. (1999). Protein backbone angle restraints from searching a database

for chemical shift and sequence homology. *J. Biomol. NMR*, **13**, 289–302.
51. Skrynnikov, N. R., Goto, N. K., Yang, D., Choy, W. Y., Tolman, J. R., Mueller, G. A. & Kay, L. E. (2000). Orienting domains in proteins using dipolar couplings measured by liquid-state NMR: differences in solution and crystal forms of maltodextrin binding protein loaded with beta-cyclodextrin. *J. Mol. Biol.* **295**, 1265–1273.
52. Brunger, A. T., Adams, P. D., Clore, G. M., DeLano, W. L., Gros, P., Grosse-Kunstleve, R. W. *et al.* (1998). Crystallography & NMR system: a new software suite for macromolecular structure determination. *Acta Crystallog. sect. D*, **54**, 905–921.
53. Cornell, W. D., Cieplak, P., Bayly, C. I., Gould, I. R., Merz, K. M., Ferguson, D. M. *et al.* (1995). A 2nd generation force-field for the simulation of proteins, nucleic-acids, and organic-molecules. *J. Am. Chem. Soc.* **117**, 5179–5197.
54. Koradi, R., Billeter, M. & Wuthrich, K. (1996). MOLMOL: a program for display and analysis of macromolecular structures. *J. Mol. Graph.* **14**, 51–55.
55. Kraulis, P. J. (1991). MOLSCRIPT: a program to produce both detailed and schematic plots of protein structures. *J. Appl. Crystallog.* **24**, 946–950.
56. Merritt, E. A. & Bacon, D. J. (1997). Raster3D: photorealistic molecular graphics. *Methods Enzymol.* **277**, 505–524.
57. Nicholls, A., Sharp, K. A. & Honig, B. (1991). Protein folding and association: insights from the interfacial and thermodynamic properties of hydrocarbons. *Proteins: Struct. Funct. Genet.* **11**, 281–296.
58. Laskowski, R. A., MacArthur, M. W., Moss, D. S. & Thornton, J. M. (1993). PROCHECK—a program to check the stereochemical quality of protein structures. *J. Appl. Crystallog.* **26**, 283–291.
59. Yap, K. L., Ames, J. B., Swindells, M. B. & Ikura, M. (2002). Vector geometry mapping. A method to characterize the conformation of helix-loop-helix calcium-binding proteins. *Methods Mol. Biol.* **173**, 317–324.
60. Jones, S. & Thornton, J. M. (1996). Principles of protein-protein interactions. *Proc. Natl Acad. Sci. USA*, **93**, 13–20.
61. Zhang, M., Tanaka, T. & Ikura, M. (1995). Calcium-induced conformational transition revealed by the solution structure of apo calmodulin. *Nature Struct. Biol.* **2**, 758–767.
62. Yap, K. L., Ames, J. B., Swindells, M. B. & Ikura, M. (1999). Diversity of conformational states and changes within the EF-hand protein superfamily. *Proteins: Struct. Funct. Genet.* **37**, 499–507.

Edited by P. E. Wright

(Received 6 January 2003; received in revised form 20 February 2003; accepted 21 February 2003)

Supplementary Material for this paper is available on Science Direct